Random Traction Yielding Transition in Epithelial Tissues

Aboutaleb Amiri,[1] Charlie Duclut,[1,2,3] Frank Jülicher,[1,4,5] and Marko Popović[1,4,5]
[1]Max Planck Institute for the Physics of Complex Systems, Nöthnitzer Strasse 38, 01187 Dresden, Germany
[2]Université Paris Cité, Laboratoire Matière et Systèmes Complexes (MSC), UMR 7057 CNRS, Paris, France
[3]Laboratoire Physico-Chimie Curie, CNRS UMR 168, Institut Curie, Université PSL, Sorbonne Université, 75005 Paris, France
[4]Cluster of Excellence Physics of Life, Technical University of Dresden, 01307 Dresden, Germany
[5]Center for Systems Biology Dresden, Pfotenhauerstrasse 108, 01307 Dresden, Germany

(Received 3 November 2022; accepted 4 October 2023; published 30 October 2023)

We investigate how randomly oriented cell traction forces lead to fluidization in a vertex model of epithelial tissues. We find that the fluidization occurs at a critical value of the traction force magnitude F_c. We show that this transition exhibits critical behavior, similar to the yielding transition of sheared amorphous solids. However, we find that it belongs to a different universality class, even though it satisfies the same scaling relations between critical exponents established in the yielding transition of sheared amorphous solids. Our work provides a fluidization mechanism through active force generation that could be relevant in biological tissues.

DOI: 10.1103/PhysRevLett.131.188401

During tissue development, many cells collectively self-organize in dynamic patterns and morphologies. Therefore, a central problem in biophysics of development is understanding the interplay of tissue mechanics and active force generation [1–6]. Cells in a tissue can generate traction forces through mechanical linkages with a substrate [7–10] and impairment of this coupling can interrupt the movement of cells as observed, for example, in cancerous spheroid assays of carcinoma and human breast organoids [11,12]. The response of biological tissues to mechanical forces is often described as that of viscoelastic active fluids [13–16]. However, recent experimental and theoretical studies have revealed complex mechanical phenomena, including jamming, glass transitions [17–22], and yield stress rheology [23,24]. These observations suggest that developing biological tissues can behave as active amorphous solids.

Recently there has been an increasing interest in the rheology of active amorphous solids [25,26]. In particular, comparing uniform shear to random forcing of particles revealed a similar nonlinear response [27]. A hallmark of sheared amorphous solids is a transition from a solid to a plastically flowing state at the yield stress Σ_c. The plastic strain rate $\dot{\gamma}$ at stress Σ above the yielding transition typically follows the Herschel-Bulkley law $\dot{\gamma} \sim (\Sigma - \Sigma_c)^{\beta}$, where $\beta \geq 1$ is the flow exponent. Yielding has recently been reported under random forcing in systems of jammed self-propelled particles [28]. This raises the question of what is the nature of the yielding transition under random forces and how it is related to the yielding transition under uniform shear. Such random yielding is relevant in the context of biological tissues, allowing them to fluidize through generation of cell traction forces, as recently reported in a study of mouse pancreas spheres [29].

Here, we investigate fundamental properties of the yielding transition through which biological tissues can be fluidized by randomly oriented cell traction forces using the vertex model of epithelial tissues [30]. Vertex model can recapitulate yielding transition under uniform shear [24] and has been used extensively to study epithelial mechanics [30]. We find that randomly oriented traction forces beyond a critical magnitude F_c fluidize the vertex model cellular network. We call this transition the "random yielding transition" (RYT) and quantify the critical exponents characterizing overall cell flow, patterns of cell rearrangements, and even the geometry of the cellular network. Interestingly, we find that some of the critical exponents differ between the RYT and the uniform shear yielding transition (YT), implying that they belong to different universality classes. Furthermore, we find that RYT critical exponents satisfy the scaling relations between exponents established for the YT [31]. These relations imply that the statistical properties of tissue dynamics and cellular geometry are not independent.

Random traction vertex model.—To explore the critical properties of RYT, we use the vertex model of epithelial tissues [30] that we extend to a spherical geometry and equip it with cell traction forces [29,32] [Fig. 1(a)]. We focus on the spherical geometry, which is ubiquitous in

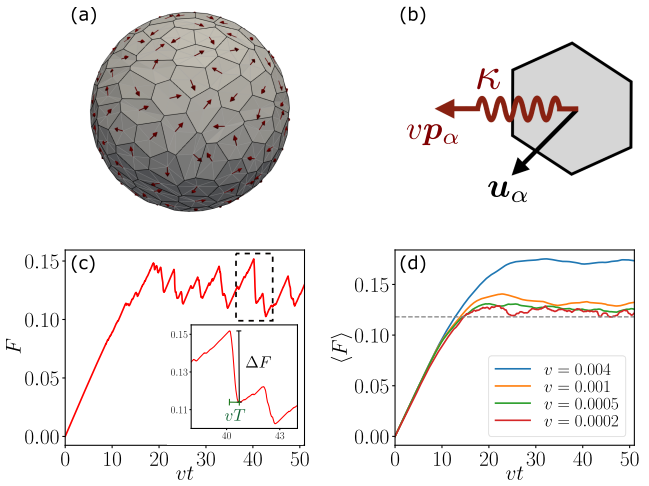

FIG. 1. (a) Spherical vertex model tissue with $N = 200$ cells with randomly oriented traction forces (red arrows). (b) Traction force is generated by extending a spring of stiffness κ at speed v in direction of the polarity $\boldsymbol{p}_\alpha$. (c) Example of the tissue traction force magnitude dynamics F as a function of spring displacement vt. (d) Dynamics of ensemble-averaged tissue traction force magnitude. As the spring extension speed v approaches the quasistatic driving limit $v \to 0$, the traction force magnitude averaged over ensemble realisations $\langle F \rangle$ converges to its critical value F_c marked by the dashed line (see SM [37]).

multicellular systems such as the early developmental stages of many tissues, including early vertebrate embryos [33,34], and early stages of organoids [29,35,36].

We represent cells as polygons outlined by straight bonds, and constrain the polygon vertices to move on a sphere of radius R. Geometry of the cellular network evolves following the dynamical equation

$$\zeta \boldsymbol{u}_m = \boldsymbol{f}_m^a - \frac{\partial W}{\partial \boldsymbol{X}_m} + \boldsymbol{f}_m^{\mathrm{n}}, \tag{1}$$

where $\boldsymbol{u}_m$ is the velocity of vertex m, ζ is the friction coefficient, $\boldsymbol{f}_m^a$ is the traction force, W is the vertex model energy function, and $\boldsymbol{f}_m^{\mathrm{n}}$ is the normal force constraining the motion of vertices on the sphere surface [see Supplemental Material (SM) [37] for details]. The vertex model energy function that accounts for cell area elasticity, cell bond tension, and cell perimeter elasticity reads

$$W = \sum_{\alpha \in \mathrm{cells}} \frac{1}{2}\left[K(A^\alpha - A_0)^2 + \Lambda L^\alpha + \Gamma (L^\alpha)^2\right]. \tag{2}$$

Here, A^α is the cell area, L^α is the cell perimeter, A_0 is the preferred cell area, K is the area stiffness, Λ is the perimeter tension magnitude, and Γ is the perimeter elastic modulus. This energy function choice describes individual cells' mechanical properties, and the tissue mechanics emerge from their collective behavior [30,38–40]. We choose units of length, force, and velocity to be $A_0^{1/2}$, $KA_0^{3/2}$ and $KA_0^{3/2}/\zeta$, respectively. The dimensionless bond tension $\bar{\Lambda} \equiv \Lambda/(KA_0^{3/2})$ is set to $\bar{\Lambda} = 0.1$. We focus on the case $\Gamma = 0$, and we show in SM that our results remain unchanged when varying the value of Γ within the solid phase of the vertex model [30,41]. Implementation details are given in the SM [37].

We consider a planar cell polarity $\boldsymbol{p}_\alpha$ that directs the traction force exerted by cell α on the surrounding matrix [Fig. 1(b)]. We initialize the direction of the cell polarity vectors $\boldsymbol{p}_\alpha$ from a uniform distribution, and evolve it following the dynamical equation

$$\frac{D\boldsymbol{p}_\alpha}{Dt} = 0, \tag{3}$$

where D/Dt denotes a corotational time derivative (see SM [37]), and we impose $|\boldsymbol{p}_\alpha| = 1$. This equation describes an infinitely persistent polarity direction in the reference frame of the cell. We define the active traction force $\boldsymbol{f}_m^a$ on a vertex m by uniformly redistributing the cell traction force $f_\alpha \boldsymbol{p}_\alpha$ of each of the abutting cells with M_α number of vertices:

$$\boldsymbol{f}_m^a = \sum_\alpha \frac{f_\alpha \boldsymbol{p}_\alpha}{M_\alpha}. \tag{4}$$

Random yielding transition.—Randomly oriented traction forces induce stresses in the vertex model network. The stress magnitude is controlled by the magnitudes of cell traction forces f_α. For small magnitudes of traction forces, we find that the elastic forces generated by the vertex model network balance the traction-induced forces, and the network remains solid. However, upon further increasing f_α, the network begins to flow through cell rearrangements. To quantitatively explore this transition, we introduce the tissue traction force magnitude $F \equiv \sum_\alpha f_\alpha/N$, which in RYT plays the role analogous to the shear stress in the YT.

Application of uniform f_α is susceptible to finite-size effects that prevent us from probing the transition. Namely, a finite-size system can by chance reach an unusually stable configuration so that the system does not flow even at high F values. To avoid this issue, we implement a model of traction forces where the attachment of a cell to the substrate moves with speed v along the vector $\boldsymbol{p}_\alpha$ and the traction force is transmitted to a spring of stiffness κ that connects the attachment and the cell [Fig. 1(b)]. Therefore, the dynamics of the traction force magnitude for a cell α follows

$$\frac{df_\alpha(t)}{dt} = -\kappa(\boldsymbol{p}_\alpha \cdot \boldsymbol{u}_\alpha - v). \tag{5}$$

Here, the term $-\kappa \boldsymbol{p}_\alpha \cdot \boldsymbol{u}_\alpha$ represents the relaxation of the force in the spring due to motion of the cell with velocity $\boldsymbol{u}_\alpha$. Limits of infinitely soft $\kappa \to 0$ and infinitely stiff

$\kappa \to \infty$ springs correspond to imposed traction forces and imposed cell center velocities, respectively. In the following, we use $\kappa = 0.01$ and vary the imposed spring extension velocity v.

An example of $F(t)$ dynamics as a function of spring displacement vt is shown in Fig. 1(c) (see also Movie 1). Initially, the cellular network responds elastically, and the traction forces grow linearly with spring displacement vt. As F increases further, the cellular network begins to yield through cell rearrangements, visible as sharp drops of F in Fig. 1(c). Finally, in the steady state, the system dynamics consist of periods of elastic loading punctuated by avalanches of cell rearrangements that are visible as sudden drops of F. Ensemble-averaged $F(t)$ for different values of v is shown in Fig. 1(d).

The observed behavior of F is reminiscent of the stress vs strain curve in sheared amorphous solids, such as metallic glasses [42], where sudden drops of stress correspond to avalanches of particle rearrangements [43]. In amorphous solids near the YT, the avalanche size, defined as the number of particle rearrangements S in an avalanche, is distributed according to a scaling law $P(S) = S^{-\tau} f(S/S_c)$, where S_c is the cutoff beyond which $P(S)$ rapidly vanishes. The cutoff is set by the correlation length ξ: $S_c \sim \xi^{d_f}$, where d_f is the avalanche fractal dimension [44]. However, approaching the YT, ξ diverges and becomes larger than the system size. Therefore, in a finite system of N cells, the cutoff S_c is set by the system size $S_c \sim N^{d_f/d}$. Furthermore, the duration of an avalanche T is expected to scale with the size as $T \sim S^{z/d_f}$, where z is the dynamical exponent [44].

To measure the avalanche size distribution, we measure drops in F in the steady state at the lowest value $v = 2 \times 10^{-4}$ we used. Then, we estimate the avalanche size corresponding to a force drop ΔF as $S \simeq N\Delta F/\kappa$. We find that the avalanche sizes are indeed power-law distributed, as shown in Fig. 2(a), with a system-size dependent cutoff. Moreover, we find $\tau = 1.35 \pm 0.11$ [45], which is consistent with the values measured in the YT of 2D elastoplastic models ($\tau = 1.25 \pm 0.05$ in Ref. [46] and $\tau = 1.36 \pm 0.03$ in Ref. [44]), of a lattice model ($\tau = 1.342 \pm 0.004$ [47]),

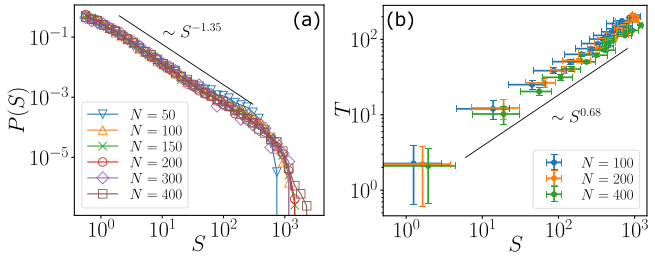

FIG. 2. Avalanche statistics. (a) Avalanche size has a power-law distribution $P(S) \sim S^{-\tau}$, with exponent $\tau = 1.35 \pm 0.11$. (b) Avalanche duration T scales with avalanche size S with exponent $z/d_f = 0.68 \pm 0.04$.

and of a finite element model ($\tau = 1.25 \pm 0.05$ [48]). We next estimated the avalanche fractal dimension $d_f = 0.75 \pm 0.15$ by finite-size scaling analysis of the avalanche distribution cutoff using $S_c \sim \langle S^3 \rangle / \langle S^2 \rangle$; see SM [37]. Finally, we find that the avalanche duration follows a power-law relationship with the avalanche size (see Fig. 2) from which we estimate $z/d_f = 0.68 \pm 0.04$.

Scaling relations connect cellular dynamics and geometry.—Exponents of YT are related through several scaling relations [44]. Here, we examine two of these relations in the context of the RYT and show that in the vertex model with random traction forces they also provide a relationship between statistics of avalanches of cell rearrangements and cell bond length distribution.

The first scaling relation follows from the fact that in the steady state $\langle \Delta F \rangle = 0$ [44], which we now briefly reproduce. Increases of F between avalanches are balanced by decreases during avalanches: $\langle |\Delta F| \rangle_+ = \langle |\Delta F| \rangle_-$. The scaling of the average decrease of F with system size can be estimated from the avalanche size distribution as $\langle |\Delta F| \rangle_- \sim \langle S \rangle / N \sim N^{(2-\tau)d_f/d-1}$. After an avalanche, F will increase until the next T1 transition. Therefore, the increases in F are determined by the network regions closest to a T1 transition. In amorphous solids the density of plastic excitations, defined as local increase in shear stress $\Delta\sigma$ required to trigger a plastic event, exhibits a pseudogap $P(\Delta\sigma) \sim \Delta\sigma^{\theta}$, with $\theta > 0$ [31,43]. Thus, the average smallest $\Delta\sigma$ in a system of size N scales as $\langle \Delta\sigma_{\min} \rangle \sim N^{-1/(1+\theta)}$ (see Ref. [44]). Since $\langle |\Delta F| \rangle_+ \sim \langle \Delta\sigma_{\min} \rangle$ it follows that

$$\tau = 2 - \frac{\theta}{1+\theta} \frac{d}{d_f}. \tag{6}$$

Using the measured values of τ and d_f, this scaling relation predicts $\theta = 0.32 \pm 0.11$.

This prediction can be tested independently by considering the statistics of the bond length distribution as follows. In a vertex model network, each T1 transition corresponds to a vanishing bond; hence, short bonds anticipate the upcoming T1 transitions. Because of cusps in the vertex model energy landscape at the onset of a T1, it was shown for the planar vertex model [24] that for short bonds the corresponding $\Delta\sigma$ is proportional to the bond length ℓ. We show that this relation also holds in the spherical vertex model tissue by measuring the additional tension Δf required to shrink a bond of length ℓ to 0; see Fig. 3(a). In general, local change in shear stress $\Delta\sigma$ will generate a proportional change in the bond tension Δf. Therefore, observed scaling of imposed Δf with bond length ℓ characterizes the scaling of $\Delta\sigma$. As a consequence, short bonds in the network for $F \leq F_c$ are distributed according to $P(\ell) \sim \ell^{\theta}$. Figure 3(b) shows the cumulative bond length distribution $C(\ell) = \int_0^{\ell} P(\ell')d\ell'$ obtained in

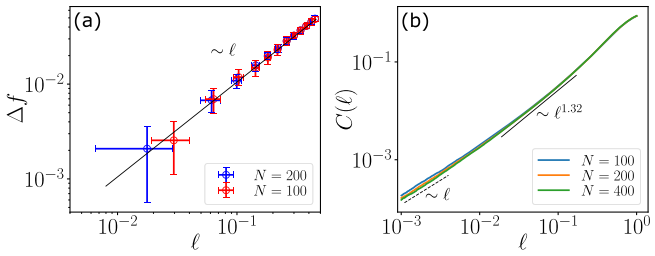

FIG. 3. Density of plastic excitations in the tissue. (a) Additional tension Δf required to collapse the bond as a function of bond length ℓ. A linear scaling is observed (solid line). (b) Cumulative bond length distribution $C(\ell)$ in the steady state for $v = 2 \times 10^{-4}$. The predicted value of the exponent $\theta \approx 0.32$ is indicated by the solid line. At low ℓ we observe a linear scaling of $C(\ell)$ (dashed line), corresponding to a constant bond length distribution, as expected at finite v and for finite system sizes.

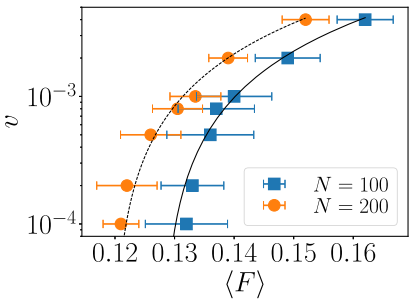

FIG. 4. Steady-state flow curve measured in spherical vertex model networks with $N = 100$ (blue squares) and $N = 200$ (orange circles). Curves show best fit to $v \sim (\langle F \rangle - F_c)^{1.41}$ for $N = 100$ (dashed line) and $N = 200$ (solid line); see SM [37] for discussion of F_c finite-size scaling.

the steady-state simulation at $v = 2 \times 10^{-4}$, where we measure bond lengths of networks at time points just after an avalanche. We find that the predicted value of the exponent θ is consistent with the bond length distribution (see also SM [37]).

The second scaling relation reflects that the flow in the vicinity of the critical point F_c is composed of avalanches of spatial extension corresponding to the correlation length $\xi \sim (F - F_c)^{-\nu}$. Since the average avalanche size scales with $S \sim S_c \sim \xi^{d_f}$ and its duration scales as $T \sim \xi^z$ the contribution of the average avalanche to the overall flow v will scale as $v \sim S/(T\xi^d) \sim (F - F_c)^{\nu(d-d_f+z)}$ [44]. This determines the exponent $\beta = \nu(z + d - d_f)$ defined by $v \sim (F - F_c)^\beta$. Here, we do not directly measure ν and instead we use an additional scaling relation $\nu = 1/(d - d_f)$ [44]. Therefore, we arrive at the relation

$$\beta = 1 + \frac{z}{d - d_f}, \tag{7}$$

which allows us to estimate $\beta = 1.41 \pm 0.098$. To test this prediction, we analyze the steady-state flow properties for various magnitudes of loading rate v as shown in Fig. 4 for two sizes $N = 100$, 200. We find a good agreement between numerical results and the value of β predicted by the scaling relation (7).

Finally, we tested whether the values of critical exponents τ, θ, d_f, and z depend on the details of the vertex model energy function by changing the value of the perimeter elastic modulus Γ. We find that for values of the dimensionless perimeter elasticity $\bar{\Gamma} = \Gamma/KA_0$ equal to 0.02 and 0.04, for which the cellular network remains in the solid phase, the critical exponents remain consistent with those reported in Table I; see SM [37].

Discussion.—We have shown that a simple model of a spherical epithelium subject to random cellular traction forces exhibits a dynamical phase transition separating the solid and flowing phases. Our work suggests that this random yielding transition is critical, similar to the well-studied yielding transition of amorphous solids under shear, but with different values of some of the critical exponents. Furthermore, we find that scaling relations between the critical exponents of the YT also hold in the RYT.

We find that the values of fractal dimension d_f and pseudogap exponent θ are clearly different from the YT values; see Table I. In particular, $d_f \approx 1.1$ in 2D YT is associated with the one-dimensional shape of avalanches of plastic events, arising from the anisotropy of the Eshelby stress propagator of individual plastic events that are aligned by the globally imposed shear axis. In the RYT we find $d_f = 0.75 \pm 0.15$, which shows that avalanches are sparser and suggests that plastic events are not aligned on the large scales.

TABLE I. The critical exponents of RYT on a sphere in comparison with reported values for YT in a 2D elastoplastic model [44].

Exponent	Expression	RYT on a sphere	YT in 2D elastoplastic model
β	$v \sim (\langle F \rangle - F_c)^\beta$	1.41 ± 0.098	1.52 ± 0.05
τ	$P(S) \sim S^{-\tau}$	1.35 ± 0.11	1.36 ± 0.03
z	$T \sim S^{z/d_f}$	0.51 ± 0.11	0.57 ± 0.03
d_f	$S_c \sim N^{d_f/d}$	0.75 ± 0.15	1.1 ± 0.04
θ	$P(\Delta\sigma) \sim \Delta\sigma^\theta$	0.32 ± 0.11	0.57 ± 0.01

It is interesting to compare the value of pseudogap exponent we found, $\theta = 0.32 \pm 0.11$, to the yielding transition in a mean-field elastoplastic model where the Eshelby stress propagator is randomly redistributed in space, thereby removing all spatial correlations [49]. In this mean-field model the pseudogap exponent $\theta = 0.39 \pm 0.02$ has been reported numerically and supported by analytical calculations. This value is consistent with our observation in RYT, while being significantly lower than the 2D YT value $\theta \approx 0.57$ [44]. It will be interesting to test whether RYT is in the mean-field yielding transition universality class by measuring and comparing other relevant critical exponents.

To test the influence of spherical geometry on the RYT we have measured the critical exponents τ, z, and z/d_f in flat 2D biperiodic vertex model simulations (see SM [37]). We found no significant difference in their values, which suggests that spherical geometry does not alter the critical behavior of the vertex model near the RYT.

The dynamical exponent z describes the dynamics of avalanche propagation $T \sim l^z$, where l is the linear extension of the avalanche. The value $z = 0.51 \pm 0.11$ we find is consistent with reported values in YT in 2D elastoplastic model $z = 0.57 \pm 0.03$ [44] and $z \simeq 0.5$ [50]. However, in the thermodynamic limit $z < 1$ cannot hold due to the finite propagation speed of elastic interactions, which requires $z \geq 2$ in overdamped systems. Indeed $z \geq 2$ was reported in a large system of disks with overdamped dynamics [28]. On the other hand, in elastoplastic models interactions are instantaneous and are not constrained by the finite propagation speed. This suggests that, for the biologically relevant system sizes we consider, the elastic interactions in our model propagate much faster than avalanches, effectively behaving as instantaneous.

The fluidization of biological tissue by random traction forces we describe in this Letter could allow the biological tissues to transition between a stable solid phase and a malleable fluid phase without the need to alter tissue density [23] or cell mechanical properties [41]. At the transition the cell dynamics become critical, which leads to large-scale correlations in cell dynamics that could be observed in experiments as a signal of RYT. Furthermore, we speculate that RYT is not limited to tissues with traction forces, but also would occur in tissues where cells generate randomly oriented active stresses instead.

We thank Matthieu Wyart for useful discussions. This work was supported by the Federal Ministry of Education and Research (Bundesministerium für Bildung und Forschung, BMBF) under Project No. 031L0160. C. D. acknowledges the support of a postdoctoral fellowship from the LabEx "Who Am I?" (ANR-11-LABX-0071) and the Université Paris Cité IdEx (ANR-18-IDEX-0001) funded by the French Government through its "Investments for the Future."

[1] G. Wayne Brodland, Vito Conte, P. Graham Cranston, Jim Veldhuis, Sriram Narasimhan, M. Shane Hutson, Antonio Jacinto, Florian Ulrich, Buzz Baum, and Mark Miodownik, Video force microscopy reveals the mechanics of ventral furrow invagination in Drosophila, Proc. Natl. Acad. Sci. U.S.A. **107**, 22111 (2010).

[2] Ray Keller, David Shook, and Paul Skoglund, The forces that shape embryos: Physical aspects of convergent extension by cell intercalation, Phys. Biol. **5**, 015007 (2008).

[3] M. C. Diaz de la Loza and B. J. Thompson, Forces shaping the Drosophila wing, Mech. Dev. **144**, 23 (2017).

[4] Litty Paul, Shu-Huei Wang, Sathiya N. Manivannan, Liana Bonanno, Sarah Lewis, Christina L. Austin, and Amanda Simcox, Dpp-induced Egfr signaling triggers postembryonic wing development in Drosophila, Proc. Natl. Acad. Sci. U.S.A. **110**, 5058 (2013).

[5] Roberto Mayor and Sandrine Etienne-Manneville, The front and rear of collective cell migration, Nat. Rev. Mol. Cell Biol. **17**, 97 (2016).

[6] Maureen Cetera, Liliya Leybova, Bradley Joyce, and Danelle Devenport, Counter-rotational cell flows drive morphological and cell fate asymmetries in mammalian hair follicles, Nat. Cell Biol. **20**, 541 (2018).

[7] Michael P Sheetz, Dan P. Felsenfeld, and Catherine G. Galbraith, Cell migration: Regulation of force on extracellular-matrix-integrin complexes, Trends Cell Biol. **8**, 51 (1998).

[8] Donald Ingber, Integrins as mechanochemical transducers, Curr. Opin. Cell Biol. **3**, 841 (1991).

[9] Olivia Du Roure, Alexandre Saez, Axel Buguin, Robert H Austin, Philippe Chavrier, Pascal Siberzan, and Benoit Ladoux, Force mapping in epithelial cell migration, Proc. Natl. Acad. Sci. U.S.A. **102**, 2390 (2005).

[10] Xavier Trepat, Michael R. Wasserman, Thomas E. Angelini, Emil Millet, David A. Weitz, James P Butler, and Jeffrey J. Fredberg, Physical forces during collective cell migration, Nat. Phys. **5**, 426 (2009).

[11] Anna Labernadie, Takuya Kato, Agustí Brugués, Xavier Serra-Picamal, Stefanie Derzsi, Esther Arwert, Anne Weston, Victor González-Tarragó, Alberto Elosegui-Artola, Lorenzo Albertazzi *et al.*, A mechanically active heterotypic e-cadherin/n-cadherin adhesion enables fibroblasts to drive cancer cell invasion, Nat. Cell Biol. **19**, 224 (2017).

[12] Kevin J. Cheung, Edward Gabrielson, Zena Werb, and Andrew J. Ewald, Collective invasion in breast cancer requires a conserved basal epithelial program, Cell **155**, 1639 (2013).

[13] Gabor Forgacs, Ramsey A. Foty, Yinon Shafrir, and Malcolm S. Steinberg, Viscoelastic properties of living embryonic tissues: A quantitative study, Biophys. J. **74**, 2227 (1998).

[14] K Venkatesan Iyer, Romina Piscitello-Gómez, Joris Paijmans, Frank Jülicher, and Suzanne Eaton, Epithelial viscoelasticity is regulated by mechanosensitive e-cadherin turnover, Curr. Biol. **29**, 578 (2019).

[15] Pierre-François Lenne and Vikas Trivedi, Sculpting tissues by phase transitions, Nat. Commun. **13**, 664 (2022).

[16] Charlie Duclut, Joris Paijmans, Mandar M. Inamdar, Carl D. Modes, and Frank Jülicher, Nonlinear rheology of cellular networks, Cells Dev. **168**, 203746 (2021).

[17] Ludovic Berthier and Jorge Kurchan, Non-equilibrium glass transitions in driven and active matter, Nat. Phys. **9**, 310 (2013).
[18] Ludovic Berthier, Elijah Flenner, and Grzegorz Szamel, How active forces influence nonequilibrium glass transitions, New J. Phys. **19**, 125006 (2017).
[19] Dapeng Bi, Xingbo Yang, M. C. Marchetti, and M. L. Manning, Motility-driven glass and jamming transitions in biological tissues, Phys. Rev. X **6**, 021011 (2016).
[20] Thomas E. Angelini, Edouard Hannezo, Xavier Trepat, Manuel Marquez, Jeffrey J. Fredberg, and David A. Weitz, Glass-like dynamics of collective cell migration, Proc. Natl. Acad. Sci. U.S.A. **108**, 4714 (2011).
[21] Eva-Maria Schoetz, Marcos Lanio, Jared A. Talbot, and M. Lisa Manning, Glassy dynamics in three-dimensional embryonic tissues, J. R. Soc. Interface **10**, 20130726 (2013).
[22] Amit Das, Srikanth Sastry, and Dapeng Bi, Controlled neighbor exchanges drive glassy behavior, intermittency, and cell streaming in epithelial tissues, Phys. Rev. X **11**, 041037 (2021).
[23] Alessandro Mongera, Payam Rowghanian, Hannah J. Gustafson, Elijah Shelton, David A. Kealhofer, Emmet K. Carn, Friedhelm Serwane, Adam A. Lucio, James Giammona, and Otger Campàs, A fluid-to-solid jamming transition underlies vertebrate body axis elongation, Nature (London) **561**, 401 (2018).
[24] Marko Popović, Valentin Druelle, Natalie A. Dye, Frank Jülicher, and Matthieu Wyart, Inferring the flow properties of epithelial tissues from their geometry, New J. Phys. **23**, 033004 (2021).
[25] Qinyi Liao and Ning Xu, Criticality of the zero-temperature jamming transition probed by self-propelled particles, Soft Matter **14**, 853 (2018).
[26] Rituparno Mandal, Pranab Jyoti Bhuyan, Pinaki Chaudhuri, Chandan Dasgupta, and Madan Rao, Extreme active matter at high densities, Nat. Commun. **11**, 1 (2020).
[27] Peter K. Morse, Sudeshna Roy, Elisabeth Agoritsas, Ethan Stanifer, Eric I. Corwin, and M. Lisa Manning, A direct link between active matter and sheared granular systems, Proc. Natl. Acad. Sci. U.S.A. **118** (2021).
[28] Carlos Villarroel and Gustavo Düring, Critical yielding rheology: From externally deformed glasses to active systems, Soft Matter **17**, 9944 (2021).
[29] Tzer Han Tan, Aboutaleb Amiri, Irene Seijo-Barandiarán, Michael F. Staddon, Anne Materne, Sandra Tomas, Charlie Duclut, Marko Popović, Anne Grapin-Botton, and Frank Jülicher, Emergent chirality in active solid rotation of pancreas spheres, bioRxiv (2022).
[30] Reza Farhadifar, Jens-Christian Röper, Benoit Aigouy, Suzanne Eaton, and Frank Jülicher, The influence of cell mechanics, cell-cell interactions, and proliferation on epithelial packing, Curr. Biol. **17**, 2095 (2007).
[31] Jie Lin, Alaa Saade, Edan Lerner, Alberto Rosso, and Matthieu Wyart, On the density of shear transformations in amorphous solids, Europhys. Lett. **105**, 26003 (2014).
[32] L. Happel, D. Wenzel, and A. Voigt, Effects of curvature on epithelial tissue–coordinated rotational movement and other spatiotemporal arrangements, Europhys. Lett. **138**, 67002 (2022).
[33] Harunobu Kagawa, Alok Javali, Heidar Heidari Khoei, Theresa Maria Sommer, Giovanni Sestini, Maria Novatchkova, Yvonne Scholte op Reimer, Gaël Castel, Alexandre Bruneau, Nina Maenhoudt *et al.*, Human blastoids model blastocyst development and implantation, Nature (London) **601**, 600 (2022).
[34] Manon Valet, Eric D. Siggia, and Ali H. Brivanlou, Mechanical regulation of early vertebrate embryogenesis, Nat. Rev. Mol. Cell Biol. **23**, 169 (2022).
[35] Jihoon Kim, Bon-Kyoung Koo, and Juergen A. Knoblich, Human organoids: Model systems for human biology and medicine, Nat. Rev. Mol. Cell Biol. **21**, 571 (2020).
[36] Chiao-Peng Hsu, Alfredo Sciortino, Yu Alice de la Trobe, and Andreas R. Bausch, Activity-induced polar patterns of filaments gliding on a sphere, Nat. Commun. **13**, 2579 (2022).
[37] See Supplemental Material at http://link.aps.org/supplemental/10.1103/PhysRevLett.131.188401, which includes theoretical and numerical details.
[38] H. Honda, H. Yamanaka, and M. Dan-Sohkawa, A computer simulation of geometrical configurations during cell division, J. Theor. Biol. **106**, 423 (1984).
[39] François Graner and James A. Glazier, Simulation of biological cell sorting using a two-dimensional extended potts model, Phys. Rev. Lett. **69**, 2013 (1992).
[40] Noriyuki Bob Ouchi, James A. Glazier, Jean-Paul Rieu, Arpita Upadhyaya, and Yasuji Sawada, Improving the realism of the cellular Potts model in simulations of biological cells, Physica A (Amsterdam) **329A**, 451 (2003).
[41] Dapeng Bi, J. H. Lopez, Jennifer M. Schwarz, and M. Lisa Manning, A density-independent rigidity transition in biological tissues, Nat. Phys. **11**, 1074 (2015).
[42] B. A. Sun, H. B. Yu, W Jiao, H. Y. Bai, D. Q. Zhao, and W. H. Wang, Plasticity of ductile metallic glasses: A self-organized critical state, Phys. Rev. Lett. **105**, 035501 (2010).
[43] Smarajit Karmakar, Edan Lerner, and Itamar Procaccia, Statistical physics of the yielding transition in amorphous solids, Phys. Rev. E **82**, 055103(R) (2010).
[44] Jie Lin, Edan Lerner, Alberto Rosso, and Matthieu Wyart, Scaling description of the yielding transition in soft amorphous solids at zero temperature, Proc. Natl. Acad. Sci. U.S.A. **111**, 14382 (2014).
[45] The uncertainty in our measurement of τ is mainly due to uncertainties in identification of avalanches at finite v; see SM [37].
[46] Mehdi Talamali, Viljo Petäjä, Damien Vandembroucq, and Stéphane Roux, Avalanches, precursors, and finite-size fluctuations in a mesoscopic model of amorphous plasticity, Phys. Rev. E **84**, 016115 (2011).
[47] Zoe Budrikis and Stefano Zapperi, Avalanche localization and crossover scaling in amorphous plasticity, Phys. Rev. E **88**, 062403 (2013).
[48] Stefan Sandfeld, Zoe Budrikis, Stefano Zapperi, and David Fernandez Castellanos, Avalanches, loading and finite size effects in 2d amorphous plasticity: Results from a finite element model, J. Stat. Mech. (2015) P02011.
[49] Jie Lin and Matthieu Wyart, Mean-field description of plastic flow in amorphous solids, Phys. Rev. X **6**, 011005 (2016).
[50] Eduardo Alberto Jagla, Different universality classes at the yielding transition of amorphous systems, Phys. Rev. E **96**, 023006 (2017).